Ain Shams Engineering Journal (2016) 7, 767–775

Ain Shams University

Ain Shams Engineering Journal

www.elsevier.com/locate/asej
www.sciencedirect.com

MECHANICAL ENGINEERING

Prediction of the aerodynamic behavior of a rounded corner square cylinder at zero incidence using ANN

Prasenjit Dey *, **Abhijit Sarkar**, **Ajoy Kumar Das**

Mechanical Engineering Department, National Institute of Technology Agartala, 799055, India

Received 12 February 2015; revised 5 November 2015; accepted 13 December 2015
Available online 13 February 2016

KEYWORDS

Square cylinder;
Rounded corner edge;
Aerodynamic prediction;
Neural Network

Abstract The aerodynamic behavior of a square cylinder with rounded corner edges in steady flow regime in the range of Reynolds number (*Re*) 5–45; is predicted by Artificial Neural Network (ANN) using MATLAB. The ANN has trained by back propagation algorithm. The ANN requires input and output data to train the network, which is obtained from the commercial Computational Fluid Dynamics (CFD) software FLUENT in the present study. In FLUENT, all the governing equations are discretized by the finite volume method. Results from numerical simulation and back propagation based ANN have been compared. It has been discovered that the ANN predicts the aerodynamic behavior correctly within the given range of the training data. It is additionally observed that back propagation based ANN is an effective tool to forecast the aerodynamic behavior than simulation, that has very much longer computational time.

1. Introduction

The fluid flow over cylindrical bluff bodies is one of the substantial subjects of extreme exploration, principally having the application in the tremendous engineering significance on heat exchangers, solar heating systems, natural circulation boilers, nuclear reactors, dry cooling towers, electronic cooling, vortex flow meters and flow dividers, probes and sensors and many more. The vast majority of these studies has been carried out by numerically and experimentally for square and circular cylinder [1–13]. The main flow regimes reported to date are; a creeping flow regime in which no flow separation takes place at the surface of the cylinder (Reynolds number, $Re < 1$). At low Reynolds numbers ($Re < 60$), a closed steady recirculation region characterized by the formation of two symmetric vortices behind the bluff body is observed. When the streamlines pass over the obstacles, due to loss of momentum at an adverse pressure gradient, separation takes place behind the obstacle symmetrically along the centerline [7]. Two different numerical methods: Lattice Boltzmann & Finite Volume, have been implemented to study the role of laminar flow past over a square cylinder for *Re* 0.5–300 [7] and found that there is very good agreement of data between the two applied methods for steady flow ($Re < 60$).

* Corresponding author. Tel.: +91 9774735514.
E-mail address: pdey.me@nita.ac.in (P. Dey).
Peer review under responsibility of Ain Shams University.

Production and hosting by Elsevier

http://dx.doi.org/10.1016/j.asej.2015.12.014

Whereas, there are a number of studies of fluid flow and heat transfer over a square or circular cylinder for Newtonian and non-Newtonian type of fluids [14–19]. In recent, a numerical study has been accomplished by Jaiman et al. [20] for a square cylinder with rounded corners in steady and unsteady flow regimes. They have reported the effect of corner radius of a square cylinder on the separation of flow, galloping etc. which is excited by freely vibration.

All the studies have been done by experimentally and numerically for high Reynolds number. The objective of the present study is to evaluate aerodynamic properties of rounded corner square cylinder at low *Re* and to predict them by using ANN. The Neural Network has a vast application to the engineering problems. The fundamental of ANN and its application on aerodynamic properties has been also studied [21–31]. In the previous list of studies, there is a study which has been conducted on a square cylinder with different radii [23] to predict the vorticity around the cylinder.

It is very clear from the literature that there is no availability of study of the prediction of aerodynamic coefficients and also the application of ANN for corner edged square cylinder at low *Re*. So the present work is carried out to predict the aerodynamic coefficient of different corner radius square cylinder (r = 0.51, 0.54, 0.59 and 0.64) with different blockage (B = 0.01, 0.05, 0.09 & 0.1) by using ANN within range of Reynolds numbers $5 \leqslant Re \leqslant 45$. The data for prediction are generated numerically by using commercial CFD software FLUENT [31]. The numerical results, those are obtained from the simulation are fed into the ANN system for training the network and the capability of ANN to predict the aerodynamic forces are thorough checked for different input parameters in MATLAB [32]. There is an abundant distinct class of structures for ANN. Feed forward back propagation Neural Network is applied in this paper as it is the most common training methods in various utilizations.

2. Geometrical configuration

The system of interest here is to study the behavior of the flow past over a square cylinder with rounded corner edges placed in a channel on the centerline (Fig. 1). The square cylinder of side D, dimensional corner radius of R and non-dimensional radius of corner '$r = R/D$' (=0.51, 0.54, 0.59 and 0.64) is held in a channel subjected to an upstream steady laminar flow of x-velocity, $u = U_\infty$ (free stream velocity). The aim is to simulate an infinitely long channel; however, the computational domain has to be finite. The distance of the upstream and the downstream boundaries from the center of the cylinder are; upstream distance from cylinder center (L_u) = $10D$ and downstream distance from cylinder center (L_d) = $40D$. The distance between the upper and lower sidewalls, H is specified according the blockage ratio (D/H = 0.05).

3. Mathematical formulation

For the incompressible, 2-D steady laminar flow across the square cylinder with cornered edges, the dimensionless forms of the continuity, the x and y components of the Navier–Stokes equation, assuming negligible dissipation, in a rectangular coordinate system are given below:

Continuity Equation:

$$\frac{\partial u}{\partial x}+\frac{\partial v}{\partial y}=0 \tag{1}$$

x-Momentum Equation:

$$\frac{\partial uu}{\partial x}+\frac{\partial vu}{\partial y}=-\frac{\partial p}{\partial x}+\frac{1}{Re}\left(\frac{\partial^2 u}{\partial x^2}+\frac{\partial^2 u}{\partial y^2}\right) \tag{2}$$

y-Momentum Equation:

$$\frac{\partial uv}{\partial x}+\frac{\partial vv}{\partial y}=-\frac{\partial p}{\partial y}+\frac{1}{Re}\left(\frac{\partial^2 v}{\partial x^2}+\frac{\partial^2 v}{\partial y^2}\right) \tag{3}$$

where $Re=\frac{\rho U_\infty D}{\mu}$ is the Reynolds number and u, v are the velocity components in x and y directions (m/s). The thermo-physical properties (viscosity, μ, density, ρ) of the streaming fluid (air) are dependent on the Reynolds number thereby solving the flow equations. The viscous and pressure forces acting on the cylinder are used to calculate the drag, lift and pressure coefficients.

The drag coefficient is given by:

$$C_D=\frac{F_D}{0.5\rho U_\infty^2 D} \tag{4}$$

where F_D is the drag force acting on the cylinder and has been computed by the unification of the pressure distribution on the four faces of the square cylinder in the direction of the fluid flow.

In order to understand the distribution of relative pressure over the body, a dimensionless known as pressure coefficient (C_p) is used and is given as:

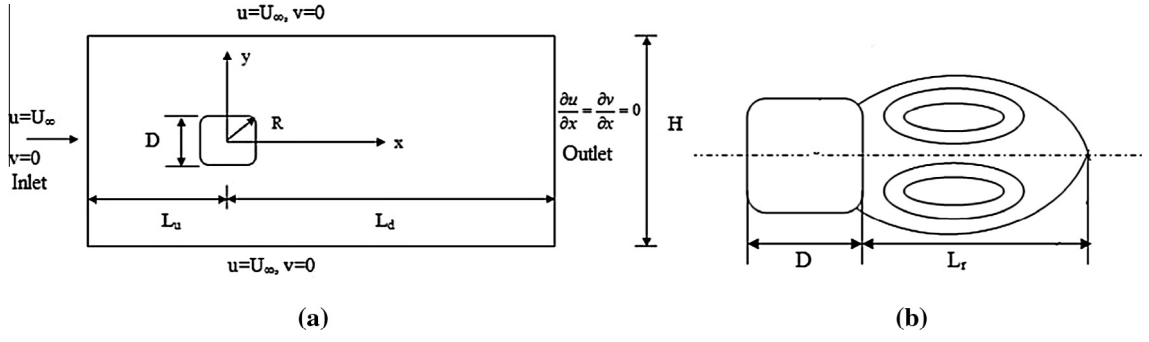

Figure 1 (a) A schematic diagram the problem description & (b) recirculation geometry.

$$C_p = \frac{p - p_\infty}{0.5\rho_\infty U_\infty^2} \quad (5)$$

where p is the pressure at the point at which pressure coefficient is being evaluated p_∞ is free stream pressure.

The dimensionless variables are defined as:

$$u = \frac{\bar{u}}{U_\infty},\ v = \frac{\bar{v}}{U_\infty},\ x = \frac{\bar{x}}{D},\ y = \frac{\bar{y}}{D},$$

$$p = \frac{\bar{p}}{\rho U_\infty^2}, \text{where } \text{‘}\bar{}\text{’ defines the dimensional variable.}$$

4. Boundary conditions

The physical boundary condition for the above discussed problem configuration are written as follows:

- The left wall of the computational domain is designed as the inlet. The “velocity inlet” boundary condition is assigned at the inlet boundary with free stream velocity, U_∞.
- The usual no-slip boundary condition is assigned for flow at the surface of the cylinder, i.e. $u = 0$; $v = 0$.
- The slip boundary condition is assigned at the upper and lower surface of the computational domain, i.e. $u = U_\infty$: $v = 0$.
- The extreme right surface of the computational domain is assigned as an outlet. The “outflow” boundary condition is employed at the exit boundary with the following conditions $\frac{\partial u}{\partial x} = \frac{\partial v}{\partial x} = 0$ of Dirichlet type Pressure boundary condition ($p = 0$).

5. CFD model

5.1. Grid structure & grid independence study

The grid structure of the computational domain used in the present investigation is shown in Fig. 2.

It is observed from Fig. 2, that the non-uniform grid structure for the whole computational domain is assigned. Grids are generated by using the grid generation package GAMBIT. The expanded view of the central block of the computational domain having the cylinder is shown in Fig. 2(b). The central block and the whole computational domain grid size are selected by studying the grid independence study. The central block which consists the cylinder has finer mesh to adequately capture the wake wall interactions in both directions and the grids becoming coarser non-uniformly toward the boundary wall. The whole computational domain is having 9 sub-blocks, in which the central block is having cylinder model with the smallest grid size of $0.07D$ of the triangular element. The grid size for the remaining blocks is increasing linearly in both x and y direction $0.3D$ to $0.5D$ from a central block to the boundary line of a quadrilateral mesh element.

In this study, three different mesh sizes (Grid1 – 15,000, Grid2 – 25,000 and Grid3 – 40,000) are adopted in order to check the mesh independent. A detailed grid independence study has been performed and results are obtained for the reattachment length (L_r) & drag coefficient (C_d) but there are no considerable changes between Grid2 and Grid3 (the results are shown in Table 1). Thus, a grid size 25,000 is found to meet the requirements of the both grid independence and computation time limit. The upstream length (L_u) & downstream length (L_d) has been selected as per the grid independence test discussed in recent work of the author Dey and Das [34,35] and assigned as $10D$ & $40D$ respectively.

5.2. Numerical details

In the present investigation, the numerical simulation is performed by using the finite volume based commercial CFD solver FLUENT 6.3 [33]. FLUENT is used to solve the governing equations which are the partial differential equations, using the control volume based technique in a collected grid system. The solver used in the present work is the pressure-based implicit method. Semi-Implicit Method for Pressure-Linked Equation (SIMPLE) is selected for the pressure–velocity coupling scheme. The pressure term is discretized under the scheme of STANDARD whereas the momentum is discretized by the second order upwind scheme. The laminar viscous model is used for the low Reynolds number considerations. The convergence criteria for the continuity and velocity are set to 10^{-5}.

6. Artificial Neural Network model

Artificial Neural Network (ANN) is an efficient computational architecture influenced by a biological neural system. An ANN consists of very simple and highly interconnected units called neurons. The neurons are interconnected with each other by links in which individual weights are passed and over which signals can pass. These neurons are arranged in a simple way, called layer & connected by a unidirectional communication path, altogether called as network architecture. The data

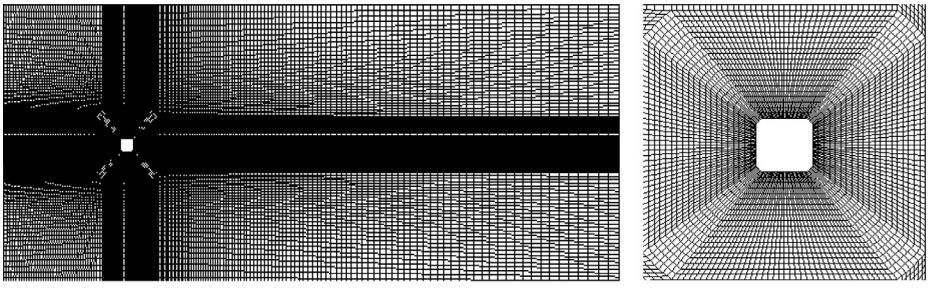

(a) (b)

Figure 2 (a) Grid Distribution of the computational domain and (b) zoomed view of the grid distribution of the cylinder.

Table 1 Study of effect of grid size for grid independency test.

No. of cells	*Re*-10		*Re*-40	
	L_r	C_d	L_r	C_d
15,000	0.47	3.10	2.55	1.41
25,000	0.50	3.26	2.70	1.72
40,000	0.50	3.27	2.70	1.72

is received by the multiple input layers & multiplied by their corresponding weights and produces the output with the help of computational node (hidden layers) that also serves as a communicator between input & output layers. The generated output may be propagated to several other neurons [30].

There is an abundant distinct class of structures for a single artificial neuron. The general mathematical formulation of a single artificial neuron could be defined as:

$$y(x) = f\left(\sum_{i=0}^{n} w_i x_i + b\right) \tag{6}$$

where x is a neuron with an input (x_0 to x_{in}) and one output y (x) and where (w_i) are weights, used to determine the appropriate weighted value for input where 'b' denotes the bias [31]. 'f' is an activation function that weights how powerful the output should be from the neuron, based on the sum of the inputs and expressed as:

$$f(x) = \frac{1}{1 + e^{-x}} \tag{7}$$

The basic feedforward network accomplishes a nonlinear transformation of input data in order to approximate the output data. The neurons are sequenced in a number of layers for a multilayer feedforward ANN, called input layer, used as a starting layer & output layer serves as an ending layer. There are numbers of hidden layers arranged in between them. There are three layers applied in the present study, namely one input layer, one hidden layer and one output layer. Connections in these kinds of a network only go forward from one layer to the next where all the neurons in each layer are connected to all the neurons in the next layer. The designed Neural Network structure 3–5–2 (3 neurons in input layer, 5 neurons in hidden layer and 2 neurons in output layer) of the present study is shown in Fig 3.

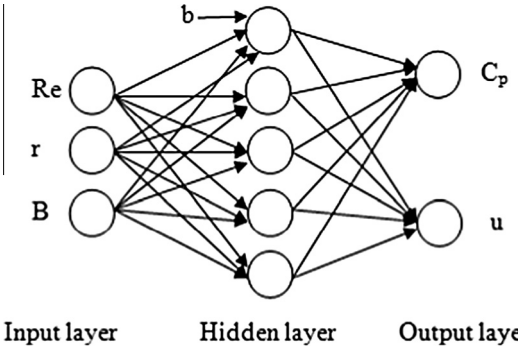

Figure 3 Schematic representation of a multilayer feedforward network consisting of three inputs, one hidden layer with five neurons and two outputs.

6.1. Training ANN

The back-propagation method is the most popular training algorithm. The input and output data are trained in ANN so that the weights can be adjusted to give the same outputs as found in the training data. The inputs (x) into a neuron are multiplied by their corresponding connection a weight (W), summed together and bias is added to the sum. This sum is transformed through a transfer function (f) to produce the required output, which may be passed to other neurons. In order to make the error smaller, the network is propagated through an input & the error is calculated and propagated back through the network by adjusting the weights simultaneously. The Levenberg–Marquardt optimization algorithm is used in the present ANN with the back propagation algorithm to accelerate the convergence condition. The termination of training process occurs when the error falls below a prescribed value or the maximum epochs is exceeded. The training data has been selected 70% of the total data and the remaining data are selected for testing. The Neural Network requires that the range of the both input and output values should between 0.1 and 0.9 due to the restriction of the sigmoid function. The numerical data evaluated in this study are normalized by the following equation:

$$x_n = \left(\frac{x_i - x_{min}}{x_{max} - x_{min}}\right) \tag{8}$$

where X_n = normalized value, X_i = actual input (or output) value, X_{max} = Maximum value of the inputs (or outputs), X_{min} = Minimum value of the inputs (or outputs).

The error between the numerical values and the ANN predicted values are presented as $R - Sq$ (R^2) & $R - Sq$ (adj) i.e. Adjusted R^2 which are expressed as:

$$R^2 = 1 - \frac{\sum_i (N_i - P_i)^2}{\sum_i (N_i - \overline{N})^2} \tag{9}$$

$$R - Sq\,(adj) = 1 - \frac{\sum_i (N_i - P_i)^2 / n - p - 1}{\sum_i (N_i - \overline{N})^2 / n - 1} \tag{10}$$

where

n = Sample Size,
p = total number of regressors in the training model.
N_i = Actual Value.
P_i = Predicted Value and
$\overline{N} = \frac{1}{n}\sum_{i=1}^{n} N_i$

7. Results and discussion

7.1. Validation of present CFD results

Since, the present work is carried out numerically; it is required to validate the present method with the published available data. So the validation is done with both the square ($r = 0.71$) and circular ($r = 0.5$) cylinder of published experimental and numerical results. The results obtained in the present investigation are compared with the published result data of [6–8,10,12] for validation. Here is also a comparison table (Tables 2 and 3) of present investigation with published results

Table 2 Comparison of L_r and C_d with the published literature values for $r = 0.71$ (square).

	$Re = 5$		$Re = 10$		$Re = 20$		$Re = 30$		$Re = 40$	
	L_r	C_d	L_r	C_d	L_r	C_d	L_r	C_d	L_r	C_d
Dhiman et al. (Numerical) [6]		4.840	0.49	3.63	1.05	2.44	1.62	1.99	2.17	1.75
Breuer et al. (Numerical) [7]			0.49	3.64	1.04	2.50	1.60	2.00	2.15	1.70
Gupta et al. (Numerical) [8]			0.40	3.51	0.90	2.45	1.40	2.06	1.90	1.86
Present study (Numerical)		4.716	0.50	3.52	1.10	2.42	1.67	2.02	2.20	1.79

Table 3 Comparison of C_d with the published literature values for $r = 0.5$ (circular).

	$Re = 10$ C_d	$Re = 20$ C_d	$Re = 30$ C_d	$Re = 40$ C_d
Tritton (Experimental) [12]		2.22		1.48
Fornberg (Numerical) [10]		2.00		1.50
Present study (Numerical)	3.22	2.24	1.75	1.51

at $Re = 10$, 20, 30 & 40 shown. The current predictions are in excellent agreement with those published data.

7.2. Prediction of drag coefficient and velocity

The variation of the drag coefficient with different blockage, corner radii and Re is presented in Table 4. The comparison of numerical and predicted ANN data of the drag coefficient & pressure drag coefficient with the Reynolds Number at various corner ratios is shown in Figs. 4(a) and 5(a). It is observed from the figure that the drag coefficient of a bluff body decreases

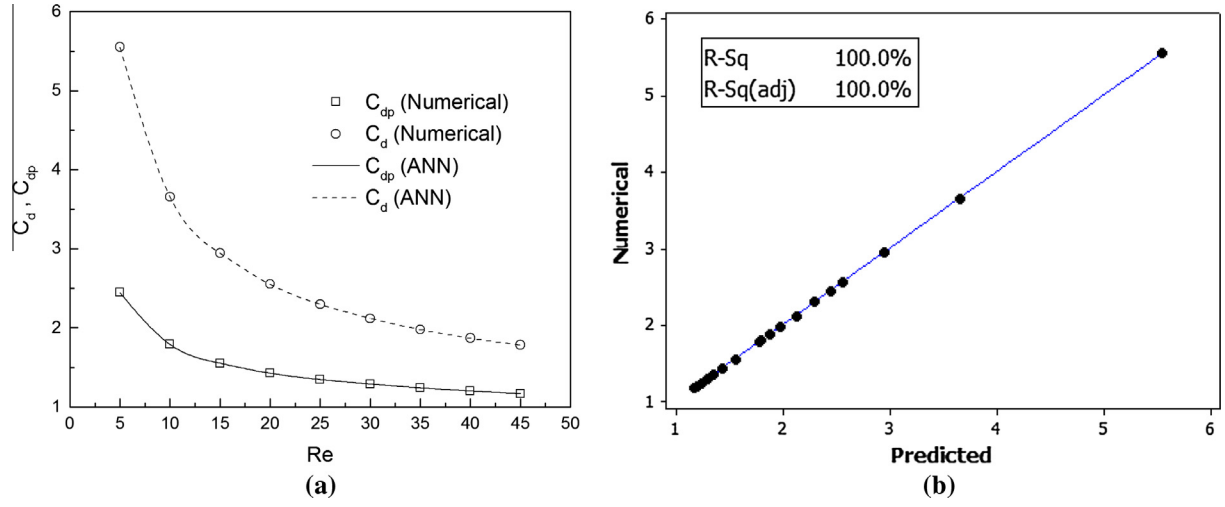

Figure 4 (a) Plot of numerical data and predicted ANN data of C_d & C_{dp} at $r = 0.64$, $B = 0.09$ & C_{dp} at $r = 0.64$, $B = 0.05$ and (b) regression plot of numerical & predicted data of C_d and C_{dp}.

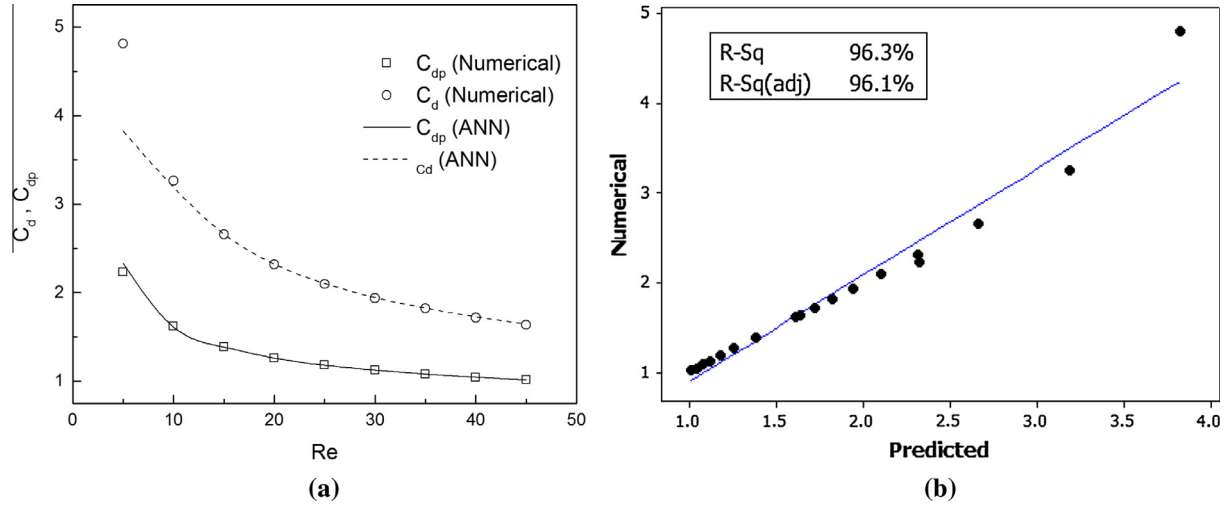

Figure 5 (a) Plot of numerical data and predicted ANN data of C_d & C_{dp} at $r = 0.59$, $B = 0.05$ and (b) regression plot of Numerical & predicted data of C_d and C_{dp}.

Table 4 Numerical values of C_d.

$B\ (=D/H)$	$r\ (=R/D)$	*Re*								
		5	10	15	20	25	30	35	40	45
0.05	0.51	4.52	3.07	2.51	2.19	1.99	1.84	1.72	1.63	1.56
0.05	0.54	4.64	3.15	2.57	2.24	2.02	1.87	1.75	1.66	1.58
0.05	0.59	4.72	3.21	2.61	2.28	2.06	1.90	1.78	1.69	1.61
0.05	0.64	4.81	3.26	2.66	2.32	2.01	1.94	1.82	1.72	1.64
0.01	0.64	4.64	3.18	2.60	2.27	2.05	1.90	1.78	1.69	1.61
0.09	0.64	5.55	3.66	2.94	2.55	2.30	2.12	1.98	1.87	1.78
0.1	0.64	5.77	3.77	3.03	2.62	2.36	2.17	2.03	1.92	1.83

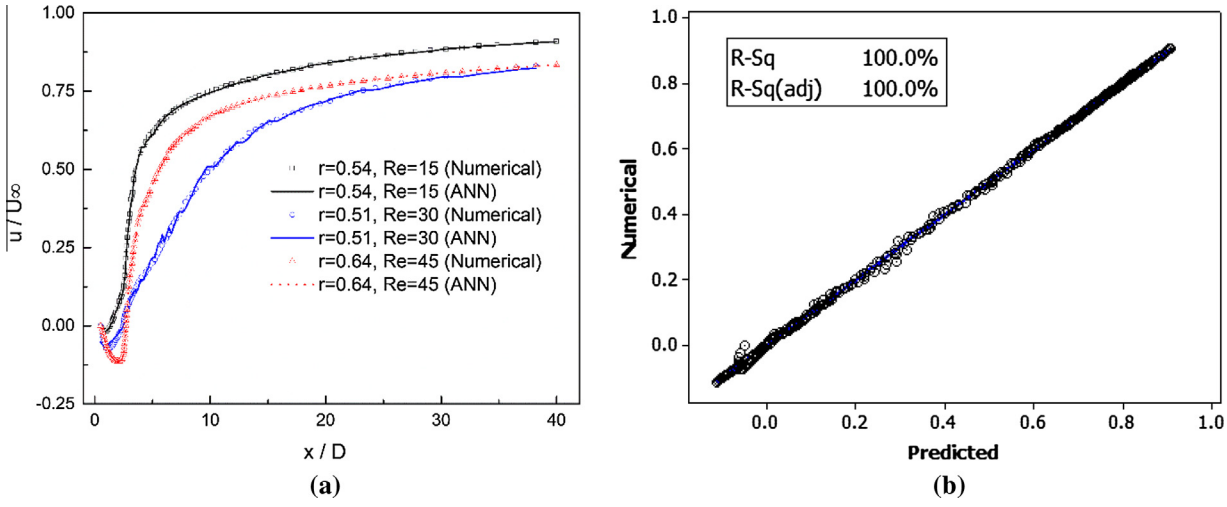

Figure 6 (a) Plot of numerical data and predicted ANN data of *x*-velocity about center line at $B = 0.05$ for $Re = 15$ & 30 and $B = 0.1$ for $Re = 45$and (b) regression plot of numerical & predicted data of *x*-velocity.

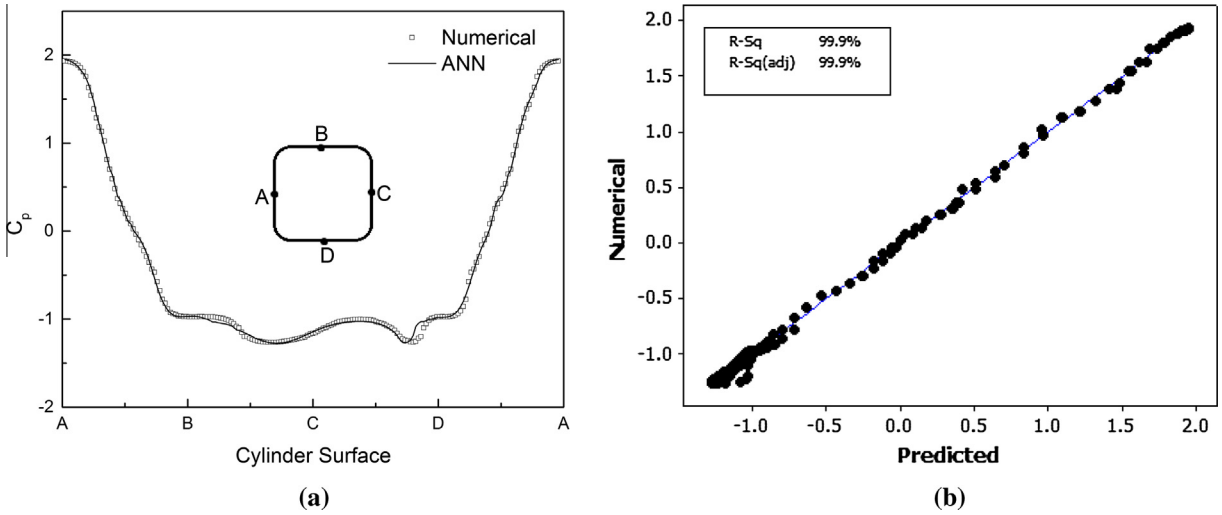

Figure 7 (a) Plot of numerical data and predicted ANN data of C_p at $Re = 5$, $B = 0.05$ & $r = 0.54$ and (b) regression plot of numerical & predicted data of C_p.

sharply with the increase of *Re* within the range of $5 \leqslant Re \leqslant 45$. Due to the increasing pressure recovery at the cylinder base; the decrease in C_d is achieved. The training and testing data are collected from the numerical analysis for $Re = 5$–45, $r = 0.51$, 0.54, 0.59 & 0.64 and $B = 0.01$, 0.05, 0.09 & 0.1. The training data are separated from the total data by keeping the particular testing data alongside. For training the network, different corner radius and different blockage values are selected within

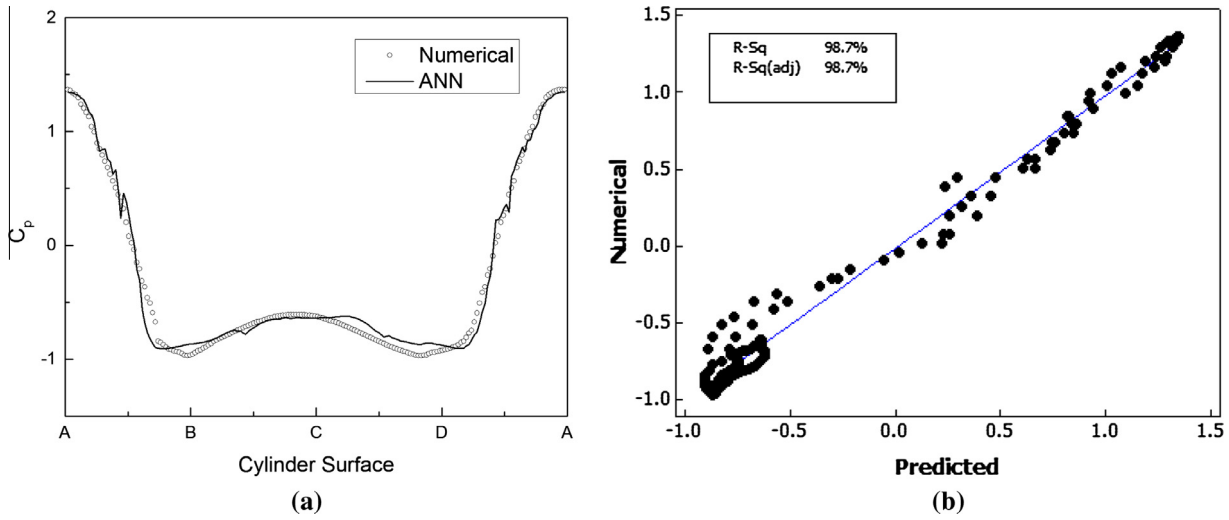

Figure 8 (a) Plot of numerical data and predicted ANN data of C_p at $Re = 15$, $B = 0.05$ & $r = 0.51$ and (b) regression plot of numerical & predicted data of C_p.

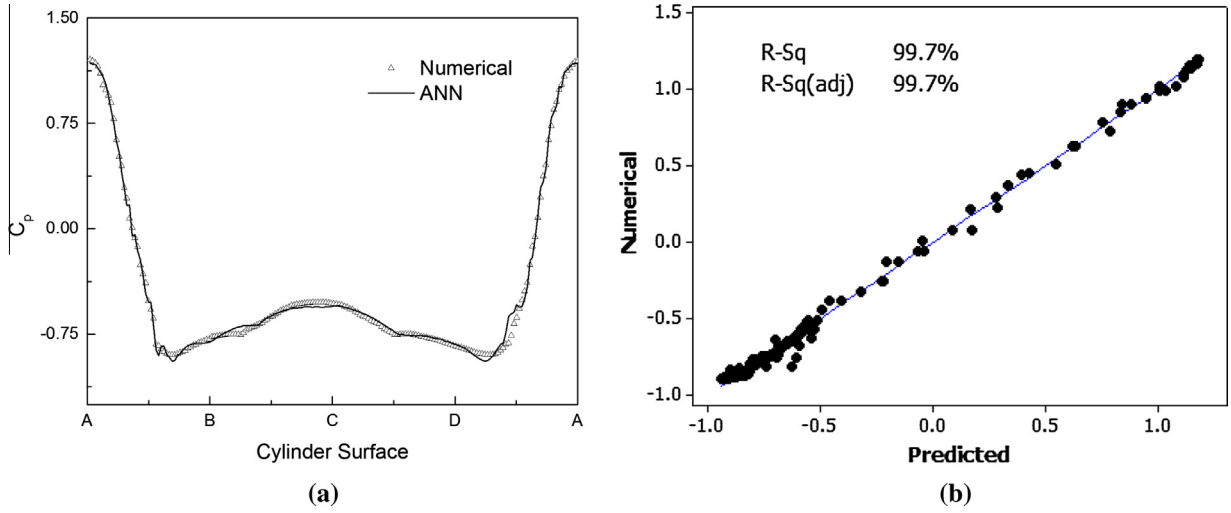

Figure 9 (a) Plot of numerical data and predicted ANN data of C_p at $Re = 30$, $B = 0.05$ & $r = 0.59$ and (b) regression plot of numerical & predicted data of C_p.

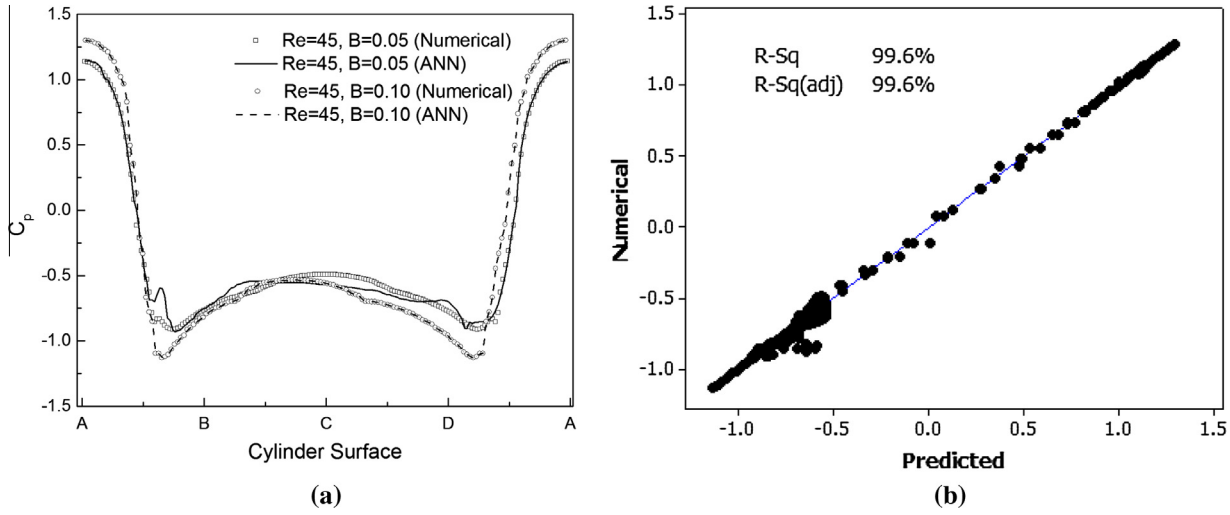

Figure 10 (a) Plot of numerical data and predicted ANN data of C_p at $r = 0.64$ and (b) regression plot of numerical & predicted data of C_p.

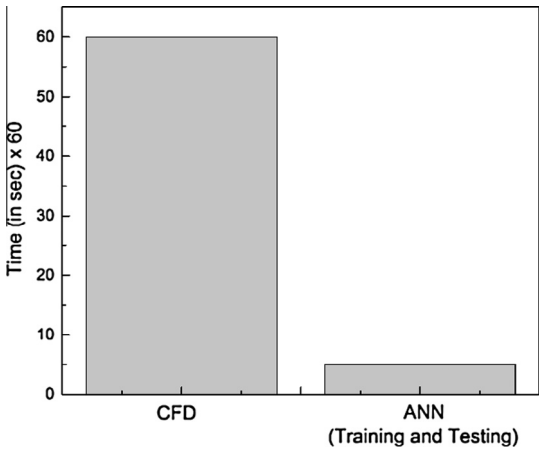

Figure 11 Bar plot of computational time of CFD and ANN.

the range of *Re* 5–45. Figs. 4(b) and 5(b) shows the variation of numerical and predicted data after testing the network, which are clearly depicted that the predicted data are in good agreement with the numerical data within the steady low Reynolds number with an adjusted *R*-square value of maximum 3.9% and a minimum of 0%. It is found that at $r = 0.64$, the ANN network predicts the best of numerical data.

The variation of numerical data & predicted data and also the regression plot of that data of the velocity in the *x*-direction in the range of *Re* $5 \leqslant Re \leqslant 45$ at different blockage ratio and different corner radius along the center line of the computational domain is shown in Fig. 6. It is clearly evident from the figure that ANN can finely predict the velocity distribution in the *x* direction for every *Re*, corner radius and different blockages.

7.3. Prediction of pressure coefficient

The pressure distribution at the different point on the cylinder surface is shown in the Figs. 7(a)–10 (a) with regression plot in 7(b)–10(b). In the present study, ANN has predicted the pressure distribution for different *Re*, corner radius and blockage. At $Re = 5$, the testing data have selected for $r = 0.54$ & $B = 0.05$ and blockage is kept same for $Re = 15$ & 30, whereas the corner radius has chosen as $r = 0.51$ & 0.59 respectively. It is found that the ANN can predict the pressure distribution at different low *Re* for different corner radius when the blockage is constant with a maximum deviation of adjusted *R*-square equals to 1.3%.

At $Re = 45$, the testing data have selected for $r = 0.6$ and $B = 0.05$ & 0.1. Here, the main objective is to find the prediction accuracy of ANN for different blockage. The distribution and variation of numerical and predicted data at $Re = 45$ are depicted in Fig. 10. It is clearly observed that the prediction data formed by ANN are in very good agreement with the numerical data also for different blockage.

The utilization of the present ANN model verified that it could provide a relation to acquire output data and have much acceptable accuracy with very little computational accomplishment time. Therefore, instead of running a case for several minutes or an hour for getting the desired results, ANN model can be used to predict that results which merely takes a few seconds or minutes. It is found that for running a single case using CFD method requires 12 times more time than ANN model (refer Fig. 11).

8. Conclusion

Back propagation Artificial Neural Network is used to predict the aerodynamic coefficients of a square cylinder with the rounded corner edge at low steady Reynolds number with different blockage and corner radius. For this purpose, series of numerical data has been developed for the cylinder model with a validation which shows a very good agreement of present result with the previously available published data. For training and testing the network, several numerical cases with combinations of input variables and output data are generated. The validity of the applied predicted methods was investigated in several cases to ensure the effectiveness to establish the results with a less permissible error. The major findings of the present study are described as follows:

- Pressure coefficient at the front stagnation point is similar for all the corner radius, whereas the value decreases toward the upper and lower surfaces of the cylinder as the flow passes over it. At the midpoint of the lower and the upper surfaces, the pressure coefficient is increasing with the increment of the corner radius which hinted that there is less pressure force acting and that pressure is increased due to the increasing of the corner radius.
- Pressure and viscous drag coefficient are mostly parallel to each other. The drag coefficient is inversely proportional to the *Re* as the drag force is inversely proportional to the inlet velocity in laminar flow. The drag coefficient is directly proportional to the '*r*'. At the lower value of '*r*', the value of drag coefficient is minimum which implies that when shape of a cylinder is becoming more curves toward the circular, it is becoming more aerodynamic & represents a monotonical behavior with corner radii.
- It can be concluded by analyzing the results that the back propagation Artificial Neural Network can predict the aerodynamic coefficients, velocity distribution accurately with minimum relative error; hence reducing the computational time in the CFD calculation while achieving acceptable accuracy.

Further, the ANN model can be utilized in higher range of *Re* for both unsteady laminar and turbulent flow regime for predicting the fluid forces and heat transfer characteristics and also for various geometrical cylinders.

References

[1] Kelkar KM, Patankar SV. Numerical prediction of vortex shedding behind a square cylinder. Int J Numer Methods Fluids 1992;14(3):327–41.
[2] Sohankar A, Davidson L, Norberg C. Numerical simulation of unsteady flow around a square two-dimensional cylinder. In: Proc 12-th Australasian fluid mechanics conference; December 1995. p. 517–20).
[3] Franke R, Rodi W, Schönung B. Numerical calculation of laminar vortex-shedding flow past cylinders. J Wind Eng Ind Aerodyn 1990;35:237–57.
[4] Sohankar A, Norberg C, Davidson L. Low-Reynolds-number flow around a square cylinder at incidence: study of blockage,

onset of vortex shedding and outlet boundary condition. Int J Numer Methods Fluids 1998;26(1):39–56.
[5] Koteswara Rao P, Sasmal C, Sahu AK, Chhabra RP, Eswaran V. Effect of power-law fluid behavior on momentum and heat transfer characteristics of an inclined square cylinder in steady flow regime. Int J Heat Mass Transfer 2011;54:2854–67.
[6] Dhiman AK, Chhabra RP, Eswaran V. Flow and heat transfer across a confined square cylinder in the steady flow regime: effect of Peclet number. Int J Heat Mass Transfer 2005;48(21):4598–614.
[7] Breuer M, Bernsdorf J, Zeiser T, Durst F. Accurate computations of the laminar flow past a square cylinder based on two different methods: lattice-Boltzmann and finite-volume. Int J Heat Fluid Flow 2000;21(2):186–96.
[8] Gupta AK, Sharma A, Chhabra RP, Eswaran V. Two-dimensional steady flow of a power-law fluid past a square cylinder in a plane channel: momentum and heat-transfer characteristics. Ind Eng Chem Res 2003;42(22):5674–86.
[9] Tritton D. Experiments on the flow past a circular cylinder at low Reynolds numbers. J Fluid Mech 1959;6(04):547–67.
[10] Dennis SCR, Chang GZ. Numerical solutions for steady flow past a circular cylinder at Reynolds numbers up to 100. J Fluid Mech 1970;42(03):471–89.
[11] Fornberg B. A numerical study of steady viscous flow past a circular cylinder. J Fluid Mech 1980;98(04):819–55.
[12] Takami H, Keller HB. Steady two-dimensional viscous flow of an incompressible fluid past a circular cylinder. Phys Fluids (1958–1988) 1969;12(12):II–51.
[13] Sen S, Mittal S, Biswas G. Steady separated flow past a circular cylinder at low Reynolds numbers. J Fluid Mech 2009;620:89–119.
[14] Dhiman A, Chhabra R, Sharma A, Eswaran V. Effects of Reynolds and Prandtl numbers on heat transfer across a square cylinder in the steady flow regime. Numer Heat Transfer, Part A: Appl 2006;49:717–31.
[15] D'Alessio SJD, Pascal JP. Steady flow of a power law fluid past a cylinder. Acta Mech 1996;117:87–100.
[16] Chhabra RP, Soares AA. Ferreira, steady non-Newtonian flow past a circular cylinder: a numerical study. Acta Mech 2004;172:1–16.
[17] Bharti RP, Chhabra RP, Eswaran V. Steady flow of power-law fluids across a circular cylinder. Can J Chem Eng 2006;84:406–21.
[18] Dhiman AK, Chhabra RP, Eswaran V. Steady flow of power-law fluids across a square cylinder. Chem Eng Res Des 2006;84:300–10.
[19] Turki S, Abbassi H, Nasrallah SB. Two-dimensional laminar fluid flow and heat transfer in a channel with a built-in heated square cylinder. Int J Therm Sci 2003;42:1105–13.
[20] Jaiman RK et al. A fully implicit combined field scheme for freely vibrating square cylinders with sharp and rounded corners. Comput Fluids 2015. http://dx.doi.org/10.1016/j.compfluid.2015.02.002.
[21] El-Bakry MY. Radial basis function neural network model for mean velocity and vorticity of capillary flow. Int J Numer Methods Fluids 2011;67(10):1283–90.
[22] Elbakry MY, El-Helly M, Elbakry MY. Neural network representation for the forces and torque of the eccentric sphere model. Trans Comput Sci 2009;3:171–83.
[23] El-Bakry MY, El-Harby AA, Behery GM. Automatic neural network system for vorticity of square cylinders with different corner radii. J Appl Math Inform 2008;26(5–6):911–23.
[24] El-Bakry MY, Radi A. Genetic programming approach for flow of steady state fluid between two eccentric spheres. Appl Rheol 2007;17(6):68210.
[25] El Bakry MY. Feed forward neural networks modeling for K–P interactions. Chaos, Solitons Fractals 2003;16(2):279–85.
[26] El-Dahshan E, Radi A, El-Bakry MY. Artificial neural network and genetic algorithm hybrid technique for nucleus–nucleus collisions. Int J Mod Phys C 2008;19(12):1787–95.
[27] Hu YC, Tsai JF. Backpropagation multi-layer perceptron for incomplete pairwise comparison matrices in analytic hierarchy process. Appl Math Comput 2006;180(1):53–62.
[28] Curry B, Morgan PH. Model selection in neural networks: some difficulties. Eur J Operat Res 2006;170(2):567–77.
[29] Maezabadi FR, Masdari M, Soltani MR. Application of artificial neural network for the prediction of pressure distribution of a plunging airfoil. In: The international conference on fluid mechanics, heat transfer and thermodynamics (FMHT2008), Paris, França; June 2008.
[30] Sreekanth S, Ramaswamy HS, Sablani SS, Prasher SO. A neural network approach for evaluation of surface heat transfer coefficient. J Food Process Preservation 1999;23(4):329–48.
[31] Kurtulus DF. Ability to forecast unsteady aerodynamic forces of flapping airfoils by artificial neural network. Neural Comput Appl 2009;18(4):359–68.
[32] Sivanandam SN, Deepa SN. Introduction to neural networks using Matlab 6.0. Tata McGraw-Hill Education; 2006.
[33] Guide FUS. Release 6.3. 26. Fluent incorporated (2005-01-06); 2006.
[34] Dey P, Das A. Steady flow over triangular extended solid attached with square cylinder – a method to reduce drag. Ain Shams Eng J 2015;6:929–38.
[35] Dey P, Das A. Numerical analysis of drag and lift reduction of square cylinder. Eng Sci Technol, Int J 2015. http://dx.doi.org/10.1016/j.jestch.2015.05.007.

Prasenjit Dey, is a Phd scholar of Mechanical Engineering Department of National Institute of Technology Agartala, India. He has completed his M-tech from NIT Agartala and joined in that institute for Phd. His research areas are Computational Fluid Dynamics, Fluid flow and heat transfer over bluff body, Optimization etc.

Dr. Abhijit Sarkar, has completed his Ph.D in manufacturing technology from National Institute of Technology Agartala, India. His research interests are in Manufacturing Technology, Advance Welding Technology, Engineering Materials and Metallurgy, Heat Transfer analysis, Optimization Techniques, Soft Computing.

Dr. Ajoy Kumar Das, is Associate Professor of Mechanical Engineering Department Of National Institute Of Technology Agartala, India. He has completed his B.E from NIT, Surathkal, India, M tech from IIT Madras, India and Ph.D from IIT Kharagpur, India. His research topics are Computational Fluid Dynamics (CFD), Heat Transfer, Thermal Power.